AN EXPERIMENTAL INVESTIGATION OF THE MOTION OF LONG BUBBLES IN INCLINED TUBES

by

Kjell H. Bendiksen

Department of Mechanics, Institute of Mathematics,

University of Oslo, Norway

Abstract: The relative motion of single long air bubbles suspended in a constant liquid flow in inclined tubes has been studied experimentally. Specially designed instrumentation, based on the difference in refractive properties of air and liquid with respect to infrared light, has been constructed and applied to measure bubble propagation rates.

A series of experiments were performed to determine the effect of tube inclination on bubble motion with liquid Reynolds and Froude numbers, and tube diameter as the most important parameters.

Particular aspects of the flow are described theoretically, and model predictions were found to compare well with observations. A correlation of bubble and average liquid velocities, based on a least squares fit to the data is suggested. Comparisons with other relevant models and data are also presented.

1. INTRODUCTION

The classical problem of determining the propagation rate of a long bubble through stagnant liquid in a vertical tube has been studied extensively by Dumitrescu (1943), Davies and Taylor (1949), and Goldsmith and Mason (1962).

When surface tension effects are negligible, and $\rho_G << \rho_L$ it is easily shown from dimensional analysis that the bubble velocity is proportional to $(gD)^{\frac{1}{2}}$. Based on the assumption of potential flow around the bubble nose, Dumitrescu obtained a series expansion for the bubble velocity, yielding a value of 0.350 for the proportionality coefficient, in excellent agreement with his own and later experimental results. Davies and Taylor independently obtained similar theoretical results (1949), but retaining the first term, only, in the series expansion, their value of 0.328 for the coefficient is somewhat too low.

Zukoski (1966) experimentally investigated the influence of viscosity and surface tension on bubble velocity for different tube inclination angles. In particular the combined effects of surface tension and inclination angle are superbly demonstrated. For all inclinations the effect of surface tension is to reduce the bubble velocity more than $(gD)^{\frac{1}{2}}$ when the tube diameter is reduced, and to finally bring the bubble to rest, altogether.

Wallis (1969) presents a review of accumulated data in terms of three dimensionless groups, representing inertia, viscous and surface tension effects.

Thus the classical problem is rather well understood for all inclinations, although an analytical solution is only available for purely inertial or viscous flow in vertical tubes.

For the more general problem of long bubble propagation through a non-stationary liquid, no theoretical solution is available. In case of laminar liquid flow with additional assumptions on bubble shape, approximate solutions may be found, Happel and Brenner (1965), but in general recourse has to be made to simple empirical correlations. For vertical tubes with a diameter of 2.59 cm Nicklin et al. (1963) found that for Reynolds numbers in the range $(8\text{-}50)\cdot 10^3$ the bubble velocity is very well correlated by

$$v_B = C_0 v_L + v_0 \qquad [1]$$

where v_0 is the rise velocity in stagnant liquid, and $C_0 \simeq 1.20$. This result may be interpreted by stating that the bubble propagates at a rate slightly less than the non-perturbed local liquid velocity at its nose, which in the actual case, assuming a 1/7 power profile would give a center velocity of about $1.22 v_L$, plus its rise velocity in stagnant liquid.

Equation [1] is well established for vertical flow, and a consequence of the hypothetical interpretation would be a weak dependence of C_0 on Re-number.

Duckler & Hubbard (1975), Singh & Griffith (1976), Bonecaze (1971), and others have applied [1] for other inclinations, but the justification is no longer evident, and actually a number of theories are in use, yielding different values for C_0 and v_0.

This is partly due to the large spread in reported experimental data, eg. for horizontal flow the values of C_0 range from 1.0 (Singh and Griffith (1976)) to 1.35 (Mattar (1974)) and $v_0/(gD)^{\frac{1}{2}}$ from 0 to 0.6. There has been a controversy regarding the proper value of v_0 for horizontal flow, Dukler & Hubbard (1975) claimes it erroneously to be zero for physical reasons.

The reported data are no better for other tube inclinations, and this certainly does not contribute to improving or restricting the large amount of fragmentary theories actually in use.

Thus, the present study has been focused on an experimental investigation of bubble propagation rate as a function of a few well defined parameters with emphasis on improved accuracy. The utilization of phototransistor technology significantly improves the precision of bubble propagation rate measurements. For each inclination angle from -30 to +90 degrees with the horizontal a series of experiments were performed, the most important parameter being Reynolds number $[5 \cdot 10^3 - 10^5]$, average liquid velocity ($\lesssim$5m/s) and tube diameter (1.9 to 5.0 cm). The test fluids applied were air and water.

The obtained results have been found to be well correlated with [1], but from a dimensional analysis of the basic equations of motion with boundary conditions, one would expect that $C_0 = C_0(D, v_L, Re, \theta)$ and $v_0^*(\sigma, v_L, \theta)$.

Finally, other experimental and theoretical results have been compared with ours, and whenever possible theoretical explanations are presented.

2. EXPERIMENTAL SET UP

2.1 Loop design

A schematic diagram of the air water loop is shown in figure 1. The test section consists of transparent acryl pipe supported by an aluminium bar that might be pivoted through angles (θ) with the horizontal of from -90 to +90 degrees. Its total length (L) was 10 m for $-30^\circ \leq \theta \leq 45^\circ$, and 7 m for $\theta \geq +60^\circ$ with inner tube diameter equal to 2.42 cm. Additional tests were performed with D=1.92 cm

and D=5.0 cm for $\theta \leq 0^{o}$ with L=4 m in all cases. Constant liquid inlet flow rate was achieved by presetting the pressure reduction and throttling valves. Additional damping of any small but rapid pressure transients, introduced for instance by the bubble entering the system, is provided by an overflow tank at the outlet.

2.2 Instrumentation

The average liquid velocity (v_L) is measured at the entrance to the test section by a De Havilland 1 inch propellometer. The bubble propagation rates (v_B^j) of its front and tail are measured over three arbitrary but preselected distances near the outlet.

For sets of emitter diodes/detector transistors are positioned exactly diametrically on the outer tube surface, and each connected to an electronic circuit as outlined in figure 2. With pure liquid flow between a transistor pair, the emitted signal attains a constant level. When the bubble arrives, the emitted light is partially reflected, and the detector (TIL 78) signal level drops, untill the bubble passes, and the level again attains its original value. This irregular signal is converted to a positive, shaped step-pulse, as indicated in figure 2. An electronic switch then sets two timers for each but the last diode/transistor pair; at the arrival of the bubble nose and tail. Those of the last pair stop all clocks, and nose and tail velocities over the actual distances may be obtained.

The signal level ratioes may be tuned to suit any particular two-phase system or tube material, provided it is transparent. To avoid stray light from other sources, transistors with maximum efficiency in the infrared range were chosen; i.e. Texas Instru-

ments TIL 32 emitter, and TIL 78 receiver with peak output/sensitivity at wavelengths of 9300 and 9150 Å, respectively.

Tilting the diode/transistor axis an angle (ϕ) with the horizontal prevents triggering on small bubbles predominantly moving near the top of the tube, and going faster than the large one in counter current liquid down flow systems. The optimal values of ϕ were found to be $\phi=30^{\circ}$ for $0\leq\theta<45^{\circ}$ and $\phi=0^{\circ}$ for $\theta\geq45^{\circ}$ or $\theta<0^{\circ}$, with separation distances (x_j) of 0.3, 0.3 and 0.6 m, respectively.

One of the signals is also used as trigger pulse for electronic blitz photographing. A General Radio 1500 P-4 Stroboscope with variable flash intensity and time delay was applied, enabling correct and flexible positioning of the bubble at the time of exposure. The tube section where photographs were taken, were enclosed in an acryl casing with walls parallel to the film, and filled with the test fluid to minimize refraction effects.

Finally, the system pressure and temperature were measured at the entrance and outlet of the test section, respectively. The void fraction in the bubble may be obtained from the photographs.

2.3 Error analysis

The static errors in the liquid velocity measurements are dominated by the flow-meter inaccuracy. In its linear range, the propellometer calibration yielded a standard deviation of ±0.3%. Two types of dynamic errors occur; firstly, rapid pressure transients, caused by either liquid or bubble inlet effects, were difficult to eliminate altogether, and may contribute to the overall uncertainty by as much as ±2%. Secondly, bubble expansion due to gravity or frictional pressure drop, or both, may introduce a bias in the liquid velocity measurements, if it is not properly accounted for.

The bubble front and tail propagation rates will differ slightly, and should be compared to the corresponding liquid velocities in front of or behind the bubble. The increased local liquid velocity at a given position (x) in the pipe due to expansion (v_L^e) may be approximated by:

$$v_L^e(x) \approx \alpha_B \frac{(\partial p/\partial x)}{p_0} L_B(x) v_B(x) \qquad [2]$$

where p_0 is a reference pressure (inlet) and $L_B(x)$ is the bubble length at a distance x from the inlet. With $L_B(x)=L_B^0 \cdot \frac{p_0}{p(x)}$, where L_B^0 is the bubble inlet length, all quantities in [2] are measured ones, and v_L^e may be obtained.

In the following, the bubble propagation rate is defined as that of the nose, and the average liquid velocity as that in front of it, given by

$$v_L = v_L^m + v_L^e$$

where v_L^m is the measured average liquid inlet velocity.

The above definitions are invariant to the direction of bubble expansion, in particular to a possible backwards expansion.

From [2] this effect is expected to be particularly important in low pressure systems with high pressure gradients. Except for low speed flow in near vertical tubes, or high speed flow (v_L>4m/s) at all inclinations, the actual expansion effects in our experiments were always below 1%, due to the relaively high system pressures applied.

The maximum static uncertainty in the bubble velocity measurement from diode/transistor couple j(Δv_B^j) may be approximated as

$$(v_B^j \pm \Delta v_B^j)/v_B^j = (1 \pm \frac{\Delta x_j}{x_j})(1 \pm \frac{\Delta t}{t_j})$$

where Δx_j is the maximum uncertainty in the bubble nose position between any two diode/transistor pairs with separation distance x_j at time t_j, and Δt_j is the instrumental time resolution.

Normally, the uncertainty, Δv_B^j, is dominated by Δx_j, and with proper focusing of the diode/transistor pair signals, this uncertainty is mainly due to changes in bubble nose shape and radial position in the tube, which are functions of velocity and inclination angle. Except for the laminar and transition to laminar regions, its maximum value was found to be $\Delta x_j < 2 \cdot 10^{-3}$ m. With the applied diode/transistor couple separation distances, upper limits on the static bubble velocity uncertainties are approximatively given by

$$\Delta v_B^j / v_B^j \lesssim 5 \cdot 10^{-3},\ 10^{-2} \quad \text{for} \quad v_L \lesssim 2 \text{ m/s} \quad \text{and} \quad 2 \text{ m/s} \lesssim v_L \lesssim 5 \text{m/s},$$

respecively.

Increased separation distances, x_j, reduces the above error, but an upper limit is imposed by the requirement that the change in bubble velocity due to expansion effects should be negligible in comparison. This enables a definition of mean bubble velocity

$$v_B = \sum_j^N v_B^j / N \qquad [3]$$

Non-stable bubbles are then excluded by requiring the separate measurements to agree within a given limit (2%) in [3]. If expansion effects are unimportant, the predominant cause of non-stable bubbles is too high or low bubble inlet pressure. The majority of such bubbles would then be either accelerating or decelerating, yielding biased results. Less than 10% of the performed experiments were discarded on these grounds.

From the above considerations a reasonable estimate of the total relative uncertainties is of the order 2-4%, depending on

the extent to which pressure transients due to inlet effects have been avoided, and a stable bubble flow achieved.

3. RESULTS

For each inclination angle a series of at least 50 tests were performed with average liquid velocity as parameter. In each experiment, when a constant liquid flow rate has been achieved, the bubble is introduced by means of pressurized air, and its velocity is measured over the distances x_j. The system pressure and average liquid velocity at the test section inlet are recorded, as well as the liquid temperature, which was normally kept about 15 ^{o}C. Bubble photographs were always taken between the last two diode/transistor pairs.

A total of 13 different inclination angles between -30 and +90 degrees were investigated for D=2.42 cm. Additional tests were performed for $\theta<0^{o}$ with inner tube diameters of 1.92 and 5.00 cm.

3.1 Bubble Propagation Data

The directly measured non-dimensional bubble propagation rates ($v_0^{\star}=v_0/\sqrt{gD}$) in stagnant liquid are presented in figure 3. These are actually averages from 8 separate tests. Due to the very large amount of data for $v_L>0$, computer analysis is required. A least squares fit (LSQ) to the relation [1] was attempted, and proved very successful, if applied over different liquid velocity intervals, as shown in table 1. Excerpts of the large amounts of v_B vs. v_L plots are shown in figures 4-6. From these plots the liquid velocity intervals with approximately constant coefficients C_0 and v_0 were determined and fed into the LSQ computer program. The LSQ values of v_0 for all inclinations with D=2.42 cm, are

presented in figure 7. Three remarkable features are observed:

i) In the lowest liqiud velocity interval, the LSQ values of v_0 are in good agreement with those from direct measurements in stagnant liquid for all θ.

ii) For high liquid velocities and $0<\theta<90^o$ v_0 decreases approximately as $v_0=v_0^v \sin\theta$, where v_0^v is the value for $\theta=90^o$.

iii) For $-30^o \lesssim \theta<0$ (liquid down flow) $v_0 \approx -|v_0(+\theta)|$ for average liquid velocities less than a critical value $v_L^c(\theta)$, and $v_0>0$ for $v_L \gtrsim v_L^c(\theta)$.

From figures 8, 9 it is evident that the bubble has turned relative to the liquid flow, its nose being aligned with the flow for $v_L \gtrsim v_L^c$.

For low liquid velocities, e.g. all but the highest interval in table 1, as might be expected from dimensional analysis, the coefficient C_0 is seen to be a complicated function of diameter (figure 10), liquid velocity, and inclination angle (table 1, figure 11). The transition to the highest C_0 is shown in figure 12 to occur for a Froude number defined as $Fr=v_L/\sqrt{gD}$, of about 3.5 for D=1.92 and 2.42 cm, relatively independent of inclination angle. Figure 10 also indicates that the Re-number is not a critical parameter in this abrupt change of C_0, although the final value of C_0 depends on it. For $Fr \gtrsim 3.5$ C_0 has a constant value of 1.19 to 1.20 for all inclinations $\theta \geq 0$ and $Re \lesssim 10^5$, as may be seen from figure 11.

For $\theta<0$ the situation appears more complicated, as shown in figure 8. For average liquid velocities below a critical value (v_L^c), both $C_0<1$ and $v_0<0$, and the bubble nose points against the liquid flow, figure 9a,d. Increasing the liquid flow rate, however, for $\theta>-30^o$ and D=2.42 cm a critical value is obtained

where the bubble turns (figure 9b-c), yielding $C_0>1$ and $v_0>0$. At still higher velocities, the bubbles are seen to behave much as for $\theta=0$, in particular $v_0\to 0$ and $C_0\to\approx 1.19$. Additional experiments with $D=1.92$ and 5.00 cm qualitatively confirms this picture, see table 1. The observed values of $v_L^c(\theta)$ are presented in figure 13.

For $\theta\lesssim -30^o$, however, the bubble dissolves into smaller bubbles before reaching the critical velocity, indicating a change in flow regime.

The void fractions (α) presented in figure 14 are those in the lowest liquid velocity interval. For $v_L\neq 0$, the film thickness varies over the first part of the bubble length due to acceleration by gravity, and the reported values of α are asymptotic ones, corresponding to the approximately constant film-thickness far down-stream.

There is a sharp increase in the uncertainty of α with increasing θ or v_L due to the centering of the bubble, and the greater difficulty in determining the exact amount of liquid at the bubble sides and top.

The standard deviations ($\Delta C_0, \Delta v_0$) in C_0 and v_0 presented in table 1, are normally less then 2-3%. The exceptions are due to applying the LSQ fits to very narrow velocity intervals. Thus, for all inclinations $\theta\geq -5^o$ the standard deviation in C_0 is less than 0.9% for the highest velocity interval.

3.2 Stability of bubble shape

Based on photographic evidence, a few observations of a more qualitative nature will be presented.

A stable bubble shape is actually never observed. Neverthe-

less, for a given liquid velocity, the film thickness at some distance down-stream from the bubble nose acquires a practically constant value, the only observable changes being a slight radial oscillation of the bubble nose, and an hydraulic jump and the production of small bubbles at its tail. For $D=2.42$ cm and all θ the average radial position of the bubble nose tip relative to the tube center is a function of liquid velocity. In the lowest liquid velocity interval, this distance is about 3/4R, decreasing to zero in the highest interval, for all θ. For low pressure systems there may be a significant increase in bubble length due to expansion.

For $\theta<0$ non-linear waves of a well defined shape were observed on the liquid film, figure 9a,d. At high Re-numbers, of course, the film surface becomes very chaotic due to turbulence for all values of θ.

3.3 Analysis

The above observations that $C_0 \to 1.19\text{-}1.20$ for Froude numbers greater than about 3.5, the conclusions i)-iii) regarding v_0, and the remarks on radial bubble nose position, all support the hypothesis that the bubble propagation rate is equal to the local liquid velocity in front of its tip, plus a gravity induced drift velocity, for all tube inclinations. The center to average liquid velocity ratio for $Re \in [4 \cdot 10^4, 10^5]$ is about 1.21. Thus equation [1] has been empirically established for all θ, but with

$$C_0 = C_0(Fr, Re, \Sigma, \theta)$$

and

$$v_0 = v_0^{\star}(Fr, Re, \Sigma, \theta) \cdot \left[gD\left(1 - \frac{\rho_G}{\rho_L}\right)\right]^{\frac{1}{2}} \qquad [4]$$

For $\theta>0$ and $Fr>3.5$ we found

$$\text{and} \qquad \begin{aligned} C_0 &\to C_0(Re,\Sigma) \\ v_0^\star &\to v_0^\star(\Sigma,\theta=90^o)\cdot\sin\theta \end{aligned} \qquad [5]$$

The first relation in [5] is a consequence of the above hypothesis and the centering of the bubble with increased v_L.

To understand the particular behaviour of $v_0^\star$, we briefly recuperate a theoretical estimate of $v_0^\star$ for horizontal flow, originally due to Brooke Benjamin (1967), and extended by D. Malnes (1982), incorporating surface tension effects.

Applying a reference system following the bubble, the continuity equation for the film under the bubble may be expressed as

$$v_F - v_B = \frac{v_L - v_B}{1-\alpha_B} \qquad [6]$$

Assuming the bubble nose tip to be a stagnation point (fig. 15a) the pressure at the center of mass (CM) far upstream may be obtained from Bernoulli as

$$P_A = P_0 - \Delta p_{\sigma_1} - \tfrac{1}{2}\rho_L(v_L-v_B)^2 + g\rho_L y_A$$

where P_0 is the (constant) bubble pressure, y_A is the distance from the radial position of the stagnation point at A to the center of mass. For case 15.a the pressure at CM in the liquid film under the bubble is given by

$$P_B = P_0 - \Delta p_{\sigma_2} + g(\rho_L y_B + \rho_G h_G)$$

where Δp_{σ_1} and Δp_{σ_2} are pressure differences due to surface tension across the bubble nose and body. Neglecting frictional effects, and assuming flat velocity profiles, an impulse ballance across the control volume A-B yields

$$\rho_L[(v_L-v_B)^2 - (1-\alpha_B)(v_F-v_B)^2] = -\Delta P \qquad [7]$$

where

$$-\Delta P = \alpha_B P_0 + (1-\alpha_B)P_B - P_A$$

Combining equations [6] and [7], Malnes obtained for $v_L=0$:

$$v_0 = \{\frac{2g(1-\alpha_B)}{1+\alpha_B}\{y_A-(1-\alpha_B)[y_B + \frac{\rho_G}{\rho_L}h_G] - \frac{1}{g\rho_L}[\Delta p_{\sigma_1}-\Delta p_{\sigma_2}(1-\alpha_B)]\}\}^{\frac{1}{2}} \qquad [8]$$

Applying Bernoulli along the free surface of the bubble nose, yields another relation between v_0 and α_B

$$g\rho_L h_G(1 - \frac{\rho_G}{\rho_L}) - \Delta p_{\sigma_3} = \tfrac{1}{2}\rho_L(v_F-v_B)^2 \qquad [9]$$

Malnes (1982) solved equations [8], [9], getting very good agreement with the experiments of Zukoski (1966) for all values of surface tension parameter, Σ.

It is an essential requirement, however, that the velocity profiles are all flat, restricting its application to stagnant liquid, only.

For high velocities, e.g. $Fr \gtrsim 3.5$, a different approach is needed. Under the idealized conditions of a fully centered bubble, figure 15.b, and arbitrary but axially symmetric flow profile, however, we note that $y_A \to y_B \to 0$, and there is no longer a net force in the x-direction due to level differences. Neglecting surface tension effects, there are no other causes for the drift velocity, and $v_0 \to 0$, as observed.

For $\theta>0$ and $v_L=0$ we may assume as a first approximation, that level and buoyancy effects act independently, and propose

$$v_0(\Sigma,\theta) = v_0^h(\Sigma,\alpha)\cos\theta + v_0^v(\Sigma,\alpha)\sin\theta \qquad [10]$$

where v_0^h is given by [8] and

$$v_0^v = v_\star^v \cdot \sqrt{gD(1-\rho_G/\rho_L)} \qquad [11]$$

Malnes incorporated surface tension effects in [11] by a semi-empirical formula:

$$v_0^v = \{gD\{(v_\star^v)^2 - \frac{1-\alpha_B}{1+\alpha_B}\cdot\Sigma\cdot[2.66 - \frac{1-\alpha_B}{\sqrt{\alpha_B}}]\}\}^{\frac{1}{2}} \qquad [12]$$

where $\Sigma=4\sigma/(g\rho_L D^2)$ and $v_\star^v=0.350$ is the non-dimensional vertical rise velocity, neglecting surface tension.

Equation [10] on dimensionless form has been solved for $v_0^\star(\Sigma,\theta)$, using the measured values of v_0^h and v_0^v, and compared with data in figure 3.

The agreement is satisfactory for $D=2.42$ cm. When surface tension effects become predominant, [10] is expected to be incorrect, but may still yield satisfactory results for small values of θ.

For $\Sigma \lesssim 3\cdot10^{-2}$ equation [10] with v_0^h and v_0^v from the analytical expressions [8] and [12], yields near identical results, but for larger values of surface tension parameter, the discrepancies increase.

For large diameter pipes, however, with moderate or negligible surface tension effects, equations [8], [10] and [12] are expected to yield reasonable estimates of v_0 for all values of $\theta>0 (v_L=0)$.

The observed limiting value of $v_0(\theta)=v_0^v\cdot\sin\theta$ for high liquid velocities follows immediately from [10], making use of the relation $v_0^h \to 0$.

The process of bubble turning

Consider the one dimensional momentum equation for the liquid film

$$\rho_L \frac{Dv_F}{dt} = -\frac{dp}{dx} - \rho_L g \sin\theta - \lambda \cdot \tfrac{1}{2}\rho_L |v_F| \cdot v_F \frac{S_w}{4A_L} + \lambda_i \tfrac{1}{2}\rho_G |v_B - v_F|(v_B - v_F)\frac{S_i}{4A_L} \qquad [13]$$

where λ, S_w and λ_i, S_i are the wall and interfacial friction factors and wetted perimeters, respectively. If a non-accelerating film flow, where frictional forces exactly balances gravity, is possible, [13] reduces to

$$\lambda \tfrac{1}{2}\rho_L (v_F^c)^2 \frac{S_w}{4A_L} = \rho_L g \sin|\theta| \qquad [14]$$

The corresponding average film speed would be given by

$$v_F^c = \left\{\frac{2\pi \sin|\theta|(1-\alpha)gD}{\lambda(\pi-\delta)}\right\}^{\frac{1}{2}} \qquad [15]$$

With α_B equal to the void fraction immediately behind the bubble nose, there may be three types of film flow.

For $v_F < v_F^c$ the flow is accelerating and the continuity equation requires $\frac{dh}{dx} < 0$, where

$$h = \frac{A_L}{b} = \frac{\pi D(1-\alpha)}{4\sin\delta}$$

is the area conserving film height. This is the normal situation up to a distance behind the bubble nose where α is large enough that [15] is satisfied with this new film thickness, it being constant from there on. For $v_F = v_F^c$ [15] applies, and $\frac{dh}{dx} = 0$. For $v_F > v_F^c$ the film flow would be decelerating and $\frac{dh}{dx} > 0$.

The continuity equation [6] and [1] yield

$$v_F - v_B = \frac{(1-C_0)v_L - v_0}{1-\alpha} \qquad [16]$$

Before the bubble has turned $C_0<1$ and $v_0<0$ and [16] imply $v_F-v_B>0$, while afterwards $C_0>1$ and $v_0>0$, and [16] requires $v_F-v_B<0$. The increase in film height with corresponding relative decrease in v_F is a thus necessary condition for the bubble to turn. Actually the film flow is strongly supercritical with respect to surface gravity/capillary waves, and there is an hydraulic jump at the bubble tail with additional loss in surface film velocity due to turbulent dissipation in the shock front. At a given v_L the bubble actually goes faster than this upper region of the film.

Finally, with increased v_L, the bubble end moving with the liquid experiences an increased drag towards the center, as for $\theta>0$, and $C_0>1$. The continuity equation [16] is then satisfied for $v_0>0$, and the bubble has turned. This process is illustrated in figure 9, in particular the film growth.

Once the film growth has commenced the turning process is very fast, indicating that the condition $C_0>1$ is already satisfied at this velocity. Thus [15] should be expected to give not only lower limit on, but also a reasonable estimate of the critical velocity. Rewriting [15] in dimensionless form, we get

$$F_B = \frac{v_F}{\left[g \sin|\theta| D(1-\alpha)^{\frac{1}{2}}\right]^{\frac{1}{2}}} \cdot \left\{\frac{\lambda(\pi-\delta)}{2(1-\alpha)^{\frac{1}{2}}}\right\}^{\frac{1}{2}} > 1$$

$$F_B = Fr^F \cdot \left\{\frac{\lambda(\pi-\delta)}{2(1-\alpha)^{\frac{1}{2}}}\right\}^{\frac{1}{2}} > 1 \qquad [17]$$

where Fr^F may be interpreted as a Froude number for the liquid film and F_B is a dimensionless number. The measured critical turning velocities and void fractions have been entered in [17], and the corresponding values of F_B are shown in figure 17, where the given uncertainties in F_B represent the observed turning interval, see figure 8. The condition $F_B>1$ is seen to be in

excellent agreement with the data.

3.4 Comparison with other data and theories

Precise, simultaneous measurements of bubble and liquid velocities are scarse. Most of the presented data were obtained for slug flow, and transient phenomena may be important. For long bubbles in stagnant liquid, however, the data of Zukoski (1966) provide a most extensive and consistent set, and a comparison of dimensionless propagation velocities, v_0^*, is presented in figure 3 for different values of surface tension parameter, Σ. The agreement is generally within 1%.

For vertical liquid up-flow, the results of Nicklin et al. (1963) of $C_0=1.20$ and $v_0=0.16$ m/s are in excellent agreement with ours. A number of others, as compiled by Nobel (1972), have reported $C_0>1.20$. For inclined and horizontal flow, the spread in data is considerable, with C_0 ranging from 0.95, Singh and Griffith (1976) to 1.32, Matter and Gregory (1974). Nickolson et al. (1978) have reported $C_0=1.196$ and $C_0=1.128$ for $D=2.58$ and 5.18 cm, respectively. These, and particularly the data of Singh and Griffith (1970), support a dependence of C_0 on Froude number, as observed by us. The reported values of $C_0>1.20$ are probably due to neglecting bubble expansion effects in low pressure systems. Except for Dukler and Hubbard (1975), there is no reported change in C_0 or v_0 with Re-number. For down-flow it is surprising that the process of bubble turning and its dynamic implications has not been previously observed or reported.

A concluding remark on two widely applied theoretical models seems appropriate. Dukler and Hubbard (1975) argues that the liquid in the slug with lateral speed less than its average liquid

velocity will be left behind, finally being shed at the bubble tail. Thus, regardless of bubble diameter, its (apparent) propagation rate would be dependent on the liquid velocity profile only, with C_0 increasing with Re-number. Secondly, for liquid down flow this argument implies $C_0>1$, contrary to experimental evidence. Our data instead shows a strong dependence of C_0 and v_0 on Froude number, with C_0 being constant over large ranges of Re-numbers. If the adopted hypothesis of Nicklin is correct, we would expect a slight decrease in C_0 with Re-number due to the decreasing maximum to average liquid velocity ratio.

In the drift flux model, eg. Zuber and Findley (1965), a basic, albeit implicit assumption is the decomposition of the flow into separate bubble units with different velocities according to their radial position in the tube. Average phase velocities may then be obtained by integration in time and radially. However, particularly the time averaging may be expected to yield poor results for a slug unit consisting of a large bubble, propagating at a radially constant speed as seen from the outside, followed by a liquid slug. Secondly, it is easily shown that integrating over the whole tube cross-section, subject to $v_B(r)$=constant, yields C_0=1.00. Allowing $\alpha\neq 0$ and $v_B(r)$=constant within the slug bubble, only, formally yields $C_0>1$, but as remarked above, the drift-flux model does not properly describe a slug unit, but rather an agglomerate of small bubbles moving independently.

A more appealing approach from a physical point of view would be to base the averaging procedure on the following assumptions:

- The slug bubble propagates at a constant velocity (v_B), independent of radial position.
- This velocity is equal to the average liquid velocity in front of the bubble, plus a possible drift velocity.

Thus, [1] is applied, but with

$$C_0 \equiv \frac{\frac{1}{A}\int \alpha \cdot v_S(r)\,dA}{[\frac{1}{A}\int \alpha dA]\cdot[\frac{1}{A}\int v_S(r)\,dA]} \qquad [18]$$

For vertical flow, the velocity profile in front of the bubble may be approximated by a power law:

$$v_S(r) = K(Re)\cdot \bar{v}_S \cdot r^{1/m}$$

where r is the fractional distance from the tube wall, $\bar{v}_S$ is the average velocity in front of the bubble, and $R_\alpha = 1-\sqrt{\bar{\alpha}}$ is the fractional distance from the tube wall to the bubble surface. For developed slug flow time averaging over a slug unit, making use of the continuity equation [6], yields $\bar{v}_S = U_G + U_L$, where U_G, U_L are the time averaged superficial velocities of gas and liquid. Integration of [18] subject to $\alpha=0$ for $r<R_\alpha$ and $\alpha=1$ for $r>R_\alpha$ yields

$$C_0 = \frac{1}{\alpha}[1-(2+\frac{1}{m})R_\alpha^{1+1/m} + (1+\frac{1}{m})R_\alpha^{2+1/m}] \qquad [19]$$

The results are summarized in table 2 for two different velocity profiles, m=7,3. As might have been expected, the obtained values of C_0 are too low, yielding a correct result only in the limit $\alpha \to 0$, where $C_0 \to 1.225$ for $m=7$. However, this value of C_0 may be considered a first order approximation, based on area averaging, in contrast to that of Dukler and Hubbard which is just wrong.

	C_0	
α	m=7	m=3
.80	1.057	1.113
.70	1.76	1.158
.60	1.094	1.201
.10	1.183	1.436

Table 2. The coefficient C_0 of [19] for vertical symmetric flow with two different profiles (m=7,3).

Note also that our model is entirely based on the above two assumptions, of which the second is not strictly correct, and it must not be confused with the drift flux model. It is not, as the latter, derived from first principles, subject to physical constraints limiting its use to flows that are basically uniform in time.

4. CONCLUSIONS

For all inclinations and velocity intervals the experimental data are well represented by [1], but with C_0 and v_0 dependent on the Reynolds- and Froude-numbers, as well as surface tension and inclination angle effects [4,5]. For liquid up flow, or horizontal flow ($\theta \geq 0$), and $Fr \lesssim 3.5$ the magnitude of C_0 ranges from 1.00 to 1.20 with one or more intervals of constant C_0 and v_0 before attaining their limits. The values of v_0 obtained form a Least Squeares fit to the data agrees very well with those of direct measurements in stagnant liquid. For $\theta > 0$ and $Fr \gtrsim 3.5$ the values of C_0 aproaches 1.19 to 1.20 for all inclinations, with $v_0 \approx v_0^v \cdot \sin\theta$. This was shown to be a consequence of increased bubble centering, which was confirmed through photographic evidence.

For liquid down flow ($\theta < 0$) and low velocities, $C_0 < 1$ and $v_0 < 0$. For any inclination, $\theta \gtrsim -30^\circ$, a critical liquid velocity is reached where the bubble turns, and propagates faster than the average liquid. A theoretical description of this process was presented, and a necessary condition for turning was found to be given by a dimensionless number [17], $F_B \geq 1$. As the second condition, $C_0 > 1$ after the bubble has turned, is always satisfied in practice if $F_B \geq 1$, the former becomes a sufficient condition as well. The experimental support of [17] is very convincing.

For $\theta \lesssim -30^{\circ}$ the bubble dissolved into smaller bubbles before turning.

For high Froude-numbers the bubble was found to behave much as for $\theta=0$, in particular $C_0 \to 1.2$ and $v_0 \to 0$.

The presented experimental data supports the hypothesis of Nicklin et al. that the bubble propagation rate is that of the liquid immediately in front of the tip of its nose, plus a possible drift velocity due to buoyancy or level effects, for all inclinations.

Particular aspects of two other theoretical models of Dukler and Hubbard (1975) and the drift flux model were presented. The first one predicts a value of C_0 from 1.25 to 1.30, increasing with Reynolds number from $3 \cdot 10^4$ to $4 \cdot 10^5$, and $v_0=0$ for horizontal flow, whereas we predict a slightly decreasing value of C_0, and a v_0 dependent on Froude-number, supported by our experimental results for $Re \lesssim 10^5$. For down-flow the former model predicts $C_0>1$, contrary to experimental evidence.

The drift flux model also proved unable to represent important aspects of slug flow, in particular its non-uniformity in time.

The proposed model based on area averaging was shown to yield too low values of C_0 for vertical flow with a reasonable velocity profile. This is another indirect support of Nicklin's hypothesis.

The comparison of our experimental results with others is not conclusive due to the large spread in reported data. For vertical flow, however, our values of C_0 and v_0 are in excellent agreement with those of Nicklin et al. For horizontal flow the agreement with Nickolson et al. is also reasonable for $Fr>3.5$. The large spread in reported data is mainly believed to be due to applying the same coefficients C_0, v_0 for all Froude-numbers, to neglecting bubble expansion effects, and to experimental errors.

ACKNOWLEDGEMENTS

The experimental part of this work was carried out at the Institute for Energy Technology, Kjeller. The author gratefully acknowledges the financial support of the Norwegian State Oil Company, Statoil.

The author would also like to express his thanks to Dr. D. Malnes for many fruitful discussions, and to Mr. S. Thue for his assistance with the instrumentation.

REFERENCES

Bonnecaze, R.H., Erskine, W. & Greskovich, E.J. 1971. Holdup and pressure drop for two-phase slug flow in inclined pipelines. Amer.Inst. of Chem.Eng.J. 17, 1109-1113.

Brooke Benjamin, T. 1968. Gravity currents and related phenomena. J.Fluid Mech. 31, 209-248.

Davies, R.M. & Taylor, G. 1949. The mechanics of large bubbles rising through extended liquids and through liquids in tubes. Proc.Roy.Soc. 200A, 375-390.

Dukler, A.E. & Hubbard, M.G. 1975. A model for gas-liquid slug flow in horizontal and near horizontal tubes. Ind.Eng.Chem.Fundam. 14, 337-346.

Dumitrescu, D.T. 1943. Strömung an einer Luftblase im senkrechten Rohr. Z.angew.Math.Mech. 23, 139-149.

Goldsmith, H.L. & Mason, S.G. 1962. The motion of single large bubbles in closed vertical tubes. J.Fluid Mech. 14, 42-58.

Happel, J & Brenner, H. 1965. Low Reynolds number Hydrodynamics with special applications to particulate Media. Prentice-Hall, Inc.

Malnes, D. 1982. Slug flow in vertical, horizontal and inclined pipes. Report IFE/KR/E-83/002 V, Institute for energy technology, Kjeller, Norway.

Mattar, L. & Gregory, G.A. 1974. Air-oil slug flow in an upward-inclined pipe - I: Slug velocity, holdup and pressure gradient. J.Can.Petr.Tech., 69-76.

Nicolson, M.K., Aziz, K & Gregory, G.A. 1978. Intermittent two-phase flow in horizontal pipes: Predictive models. Can.J.Chem.Engng. 56, 653-663.

Nicklin, D.J., Wilkes, J.O. & Davidson, J.F. 1962. Two-phase flow in vertical tubes. Trans.Instn.Chem.Engrs. 40, 61-68.

Nobel, L. 1972. The slug flow equation. Report EUR 4811e.

Singh, G. & Griffith, P. 1970. Determination of the pressure drop optimum pipe size for a two-phase slug flow in an inclined pipe. J.Engng. for Industry, 717-725.

Singh, G. & Griffith, P. 1976. Down sloping inclined pipe pressure drop and holdup. ASME Report 76-Pet-29.

Wallis, G.B. 1969. One dimensional two-phase flow. McGraw-Hill, New York.

Zuber, N. & Findlay, J.A. 1965. Average volumetric consentrations in two-phase flow systems. J.Heat Transfer, 453-468.

Zukoski, E.E. 1966. Influence of viscosity, surface tension, and inclination angle on motion of long bubbles in closed tubes. J.Fluid Mech. 25, 821-837.

D	θ	C	v_0	Δ_{C_0}	Δ_{v_0}	$[v_L^{min}, v_L^{max}]$	$[Re^{min}, Re^{max}]$	N
(cm)	(o)	-	m/s	-	(m/s)	(m/s)	$\cdot 10^4$	-
1.92	-5	.984	-.114	.092	.054	.30-0.85	.5-1.4	6
1.92	-5.	1.024	+.149	.032	.048	1.00-1.75	1.6-2.8	11
1.92	-5	1.115	.074	.006	.022	1.75-5.	2.8-8.0	11
1.92	0.	1.045	.171	.014	.014	.30-1.50	.5-2.6	26
1.92	0.	1.170	.000	.008	.027	1.60-4.40	2.7-7.1	15
2.42	-30.	.944	-.256	.011	.012	.30-2.20	.6-4.6	15
2.42	-15.	.983	-.246	.008	.010	.30-2.40	.6-5.0	26
2.42	-15.	1.073	+.086	.039	.111	2.40-3.20	5.0-6.7	10
2.42	-15.	1.141	+.047	.036	.133	3.40-4.20	7.1-8.7	5
2.42	-15.	1.18	0.	-	-	4.20-5.	8.7-10.4	2
2.42	-5.	.976	-.193	.029	.024	.30-1.25	.6-2.5	19
2.42	-5.	1.084	+.086	.053	.094	1.40-2.10	2.9-4.4	12
2.42	-5.	1.146	.000	.009	.026	2.15-4.40	4.4-9.2	26
2.42	-2.	.985	-.190	.08	.030	.30-.70	.6-1.3	15
2.42	-2.	1.084	+.100	.028	.035	.88-1.60	1.8-3.3	16
2.42	-2.	1.16	0.	.006	.017	1.60-4.15	3.3-8.6	28
2.42	0.	1.009	.181	.016	.013	.30-1.10	.6-2.3	27
2.42	0.	1.067	.145	.072	.113	1.20-1.70	2.5-3.5	11
2.42	0.	1.171	-.004	.005	.013	1.73-3.60	3.6-7.5	37
2.42	0.	1.188	.000	.005	.015	3.70-5.	7.7-10.4	17
2.42	+2.	1.008	.191	.016	.011	.30-1.10	.6-2.3	28
2.42	+2.	1.068	.140	.068	.091	1.10-1.55	2.5-3.2	8
2.42	+2	1.190	.000	.004	.012	1.60-4.30	3.3-8.8	35
2.42	+5.	.999	.223	.016	.013	.30-1.10	.6-2.3	18
2.42	+5.	1.090	.160	.054	.070	1.20-1.80	2.5-3.7	11
2.42	+5.	1.194	.025	.004	.010	1.85-5.	3.8-10.4	36
2.42	+15.	1.023	.214	.04	.03	.40-1.10	.7-2.3	6
2.42	+15.	1.105	.180	.060	.080	1.15-1.85	2.5-3.8	11
2.42	+15.	1.191	.044	.005	.01	1.90-5.	3.9-10.4	40
2.42	+30.	1.046	.230	.029	.020	.40-1.00	.7-2.1	15
2.42	+30.	1.123	.180	.055	.075	1.10-1.60	2.3-3.3	7
2.42	+30.	1.190	.086	.003	.008	1.70-4.30	3.5-8.8	33
2.42	+45.	1.097	.234	.012	.011	.30-1.60	.6-3.3	23
2.42	+45.	1.195	.120	.017	.035	1.70-3.60	3.5-5.4	12
2.42	+60.	1.120	.212	.012	.012	.40-1.60	.7-3.3	25
2.42	+60.	1.199	.135	.007	.023	1.80-5.	3.7-10.4	12
2.42	+75.	1.135	.200	.012	.012	.30-1.60	.6-3.3	20
2.42	+75.	1.190	.155	.006	.017	1.60-5.	3.3-10.4	15
2.42	+90.	1.196	.154	.002	.005	.30-5.	.6-10.4	64
5.00	-5.	.98	-.41	.02	.03	.15~1.15	.6~5.0	13
5.00	0.	1.00	.33	.04	.02	.15~1.00	.6~4.3	17

Table 1. The coefficients C_0 and v_0 with standard deviations (Δ_{C_0}, Δ_{v_0}) obtained from a least squares fit of the experimental data to [1] for different average liquid velocity intervals (v_L^{min}, v_L^{max}), inclination angles (θ) and tube diameters (D). (N is the number of successful experiments).

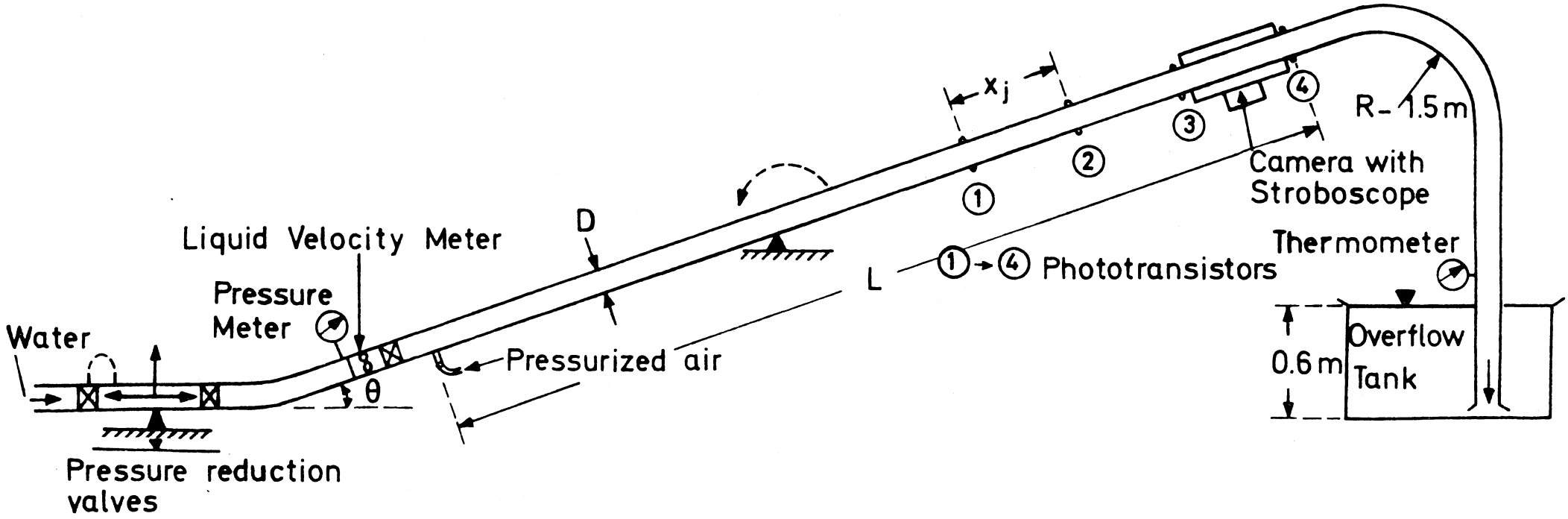

Figure 1. Schematic diagram of the test-section.

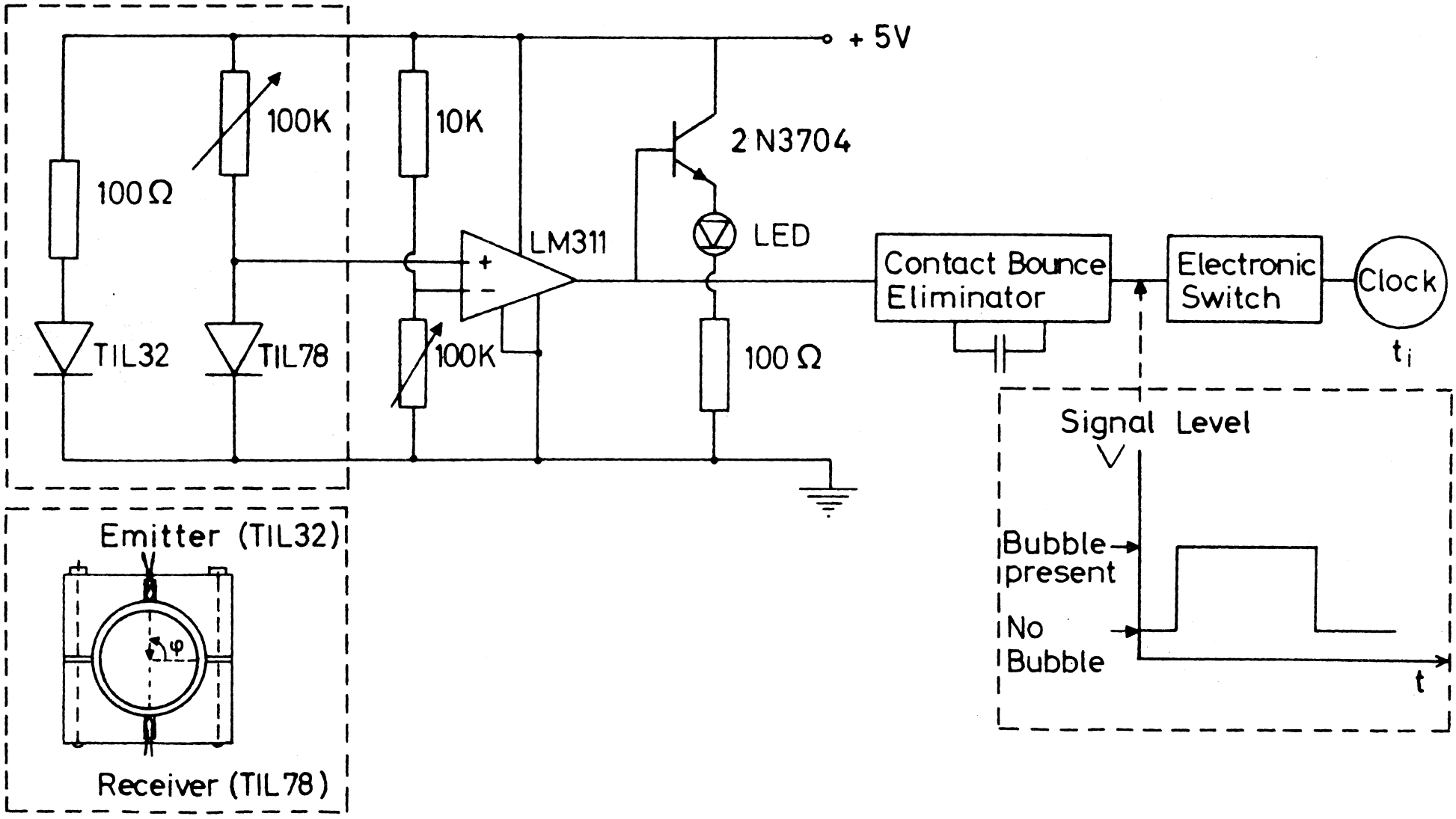

Figure 2. Schematic diagram of the bubble velocity meter.

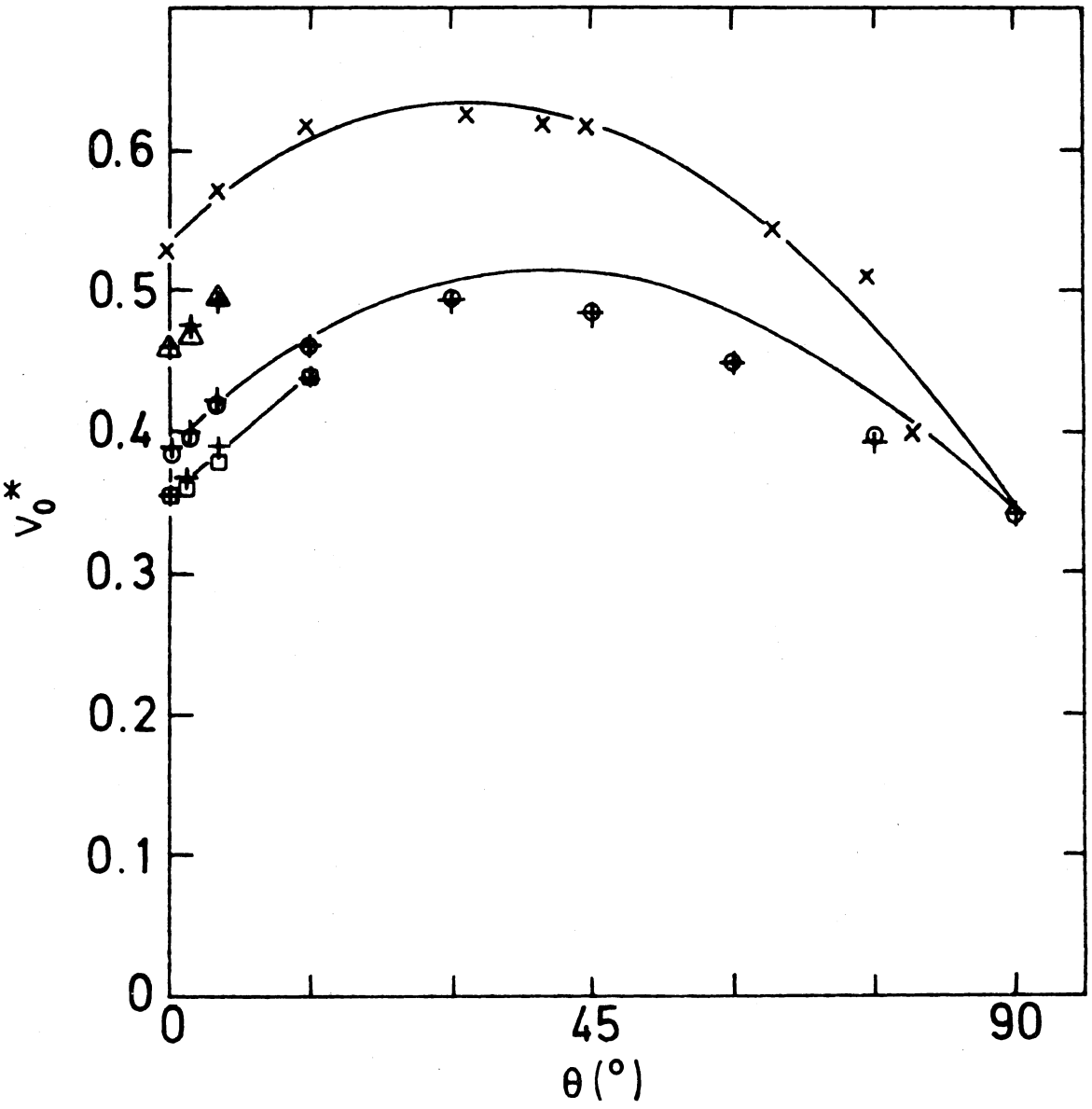

Figure 3. Dimensionless bubble propagation velocity in stagnant liquid vs inclination angle for different surface tension parameters (—— Equation [10], Our data: □,o, $\Delta\Sigma$=0.064, 0.042, 10^{-2}. Data of Zukoski (1965): ×$\Sigma=10^{-3}$, +$\Sigma=10^{-2}$, 0.042, 0.064).

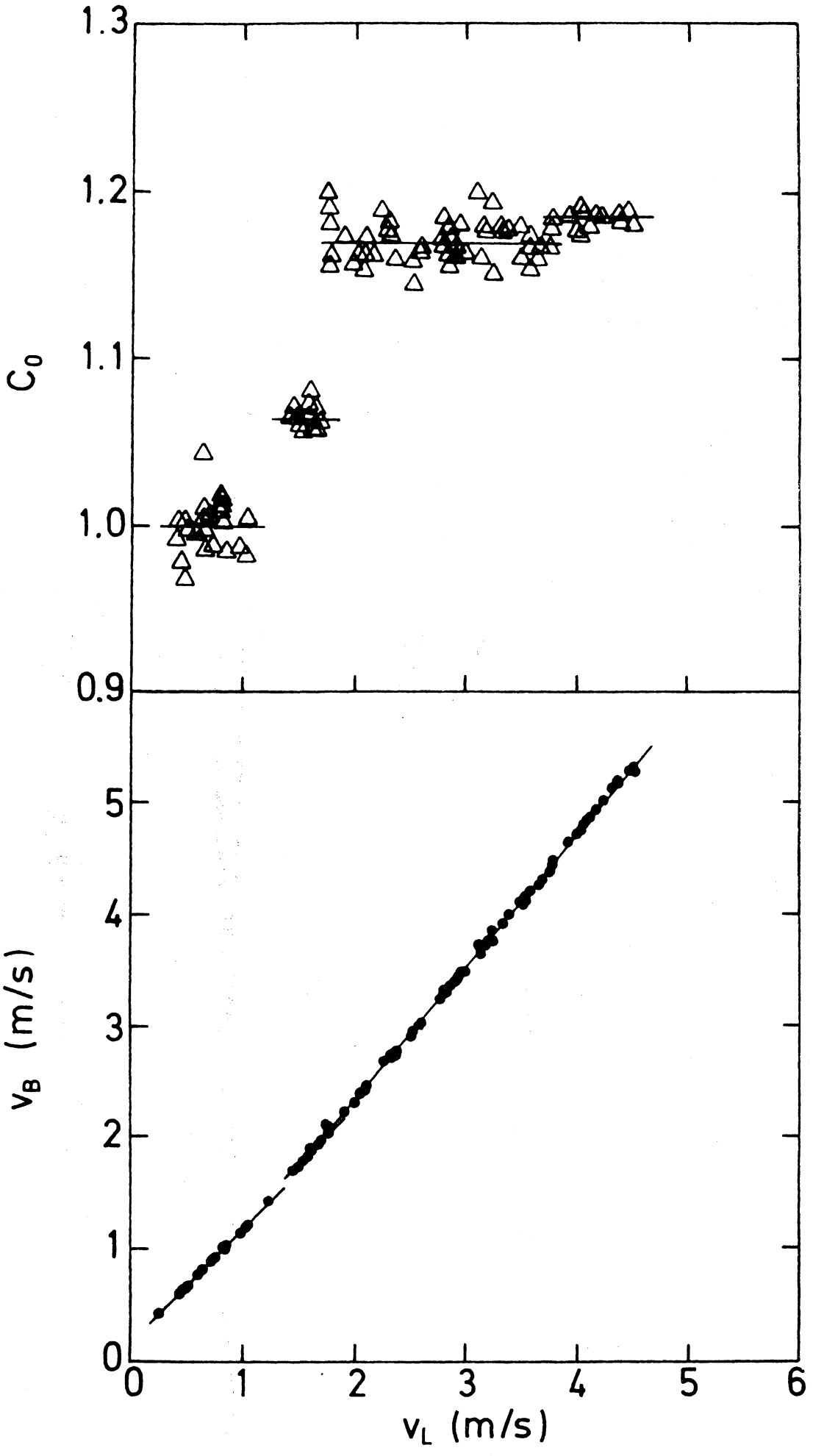

Figure 4. Measured bubble velocity and C_0 [1] vs average liquid velocity ($\theta=0^o$, D=2.42 cm).

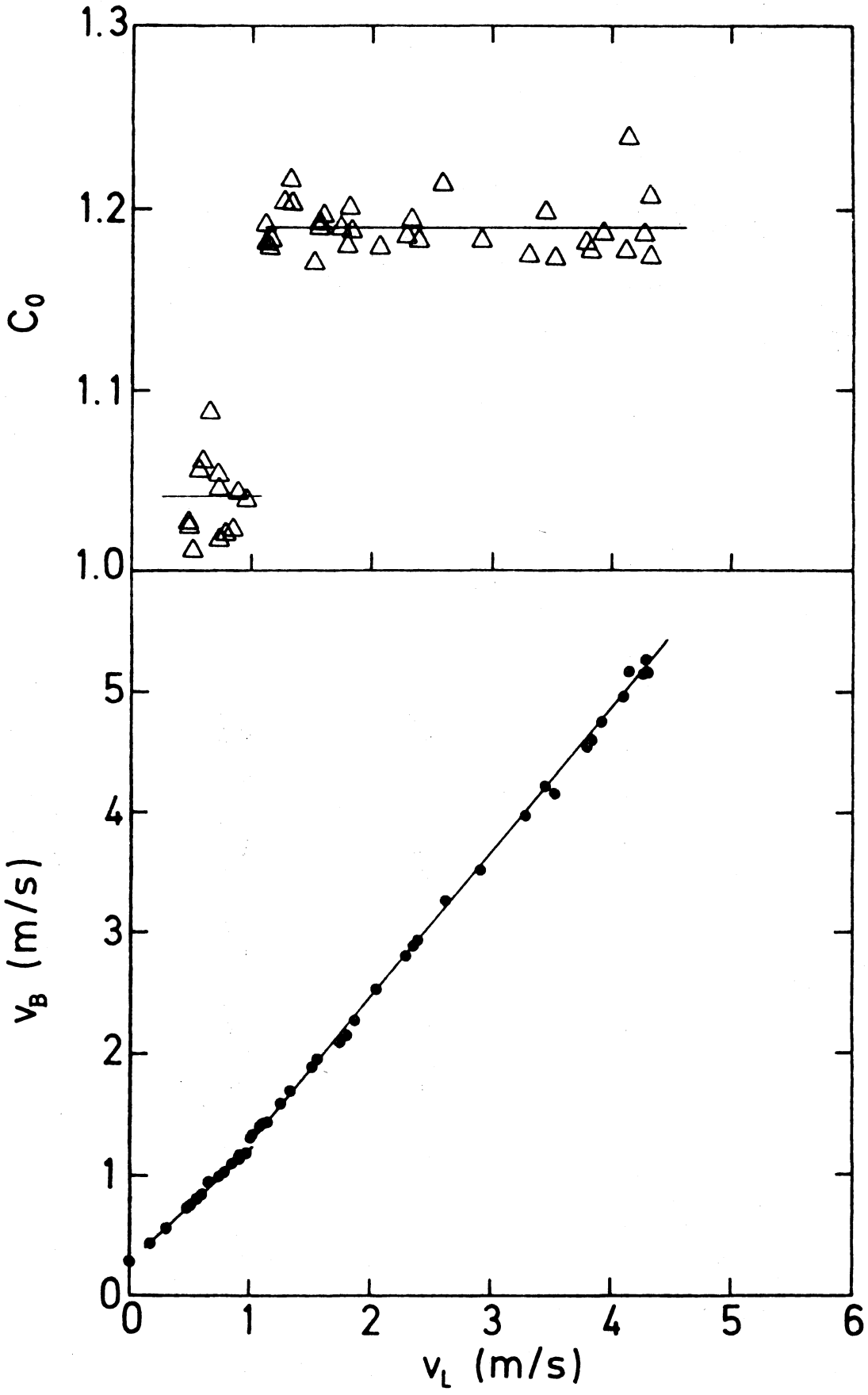

Figure 5. Measured bubble velocity and C_0 [1] vs average liquid velocity ($\theta=30^{o}$, D=2.42 cm).

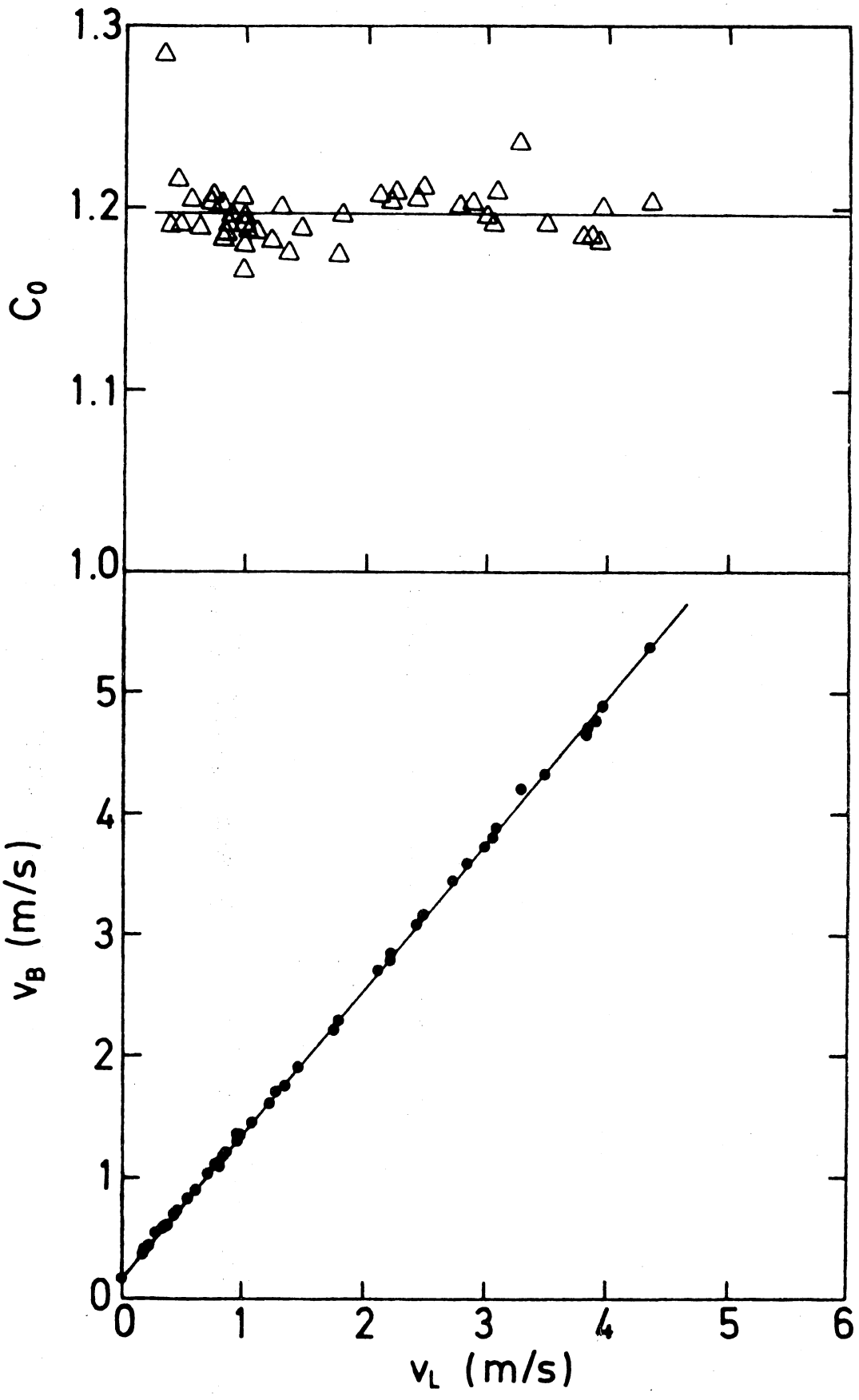

Figure 6. Measured bubble velocity and C_0 [1] vs average liquid velocity ($\theta=90^{o}$, D=2.42 cm).

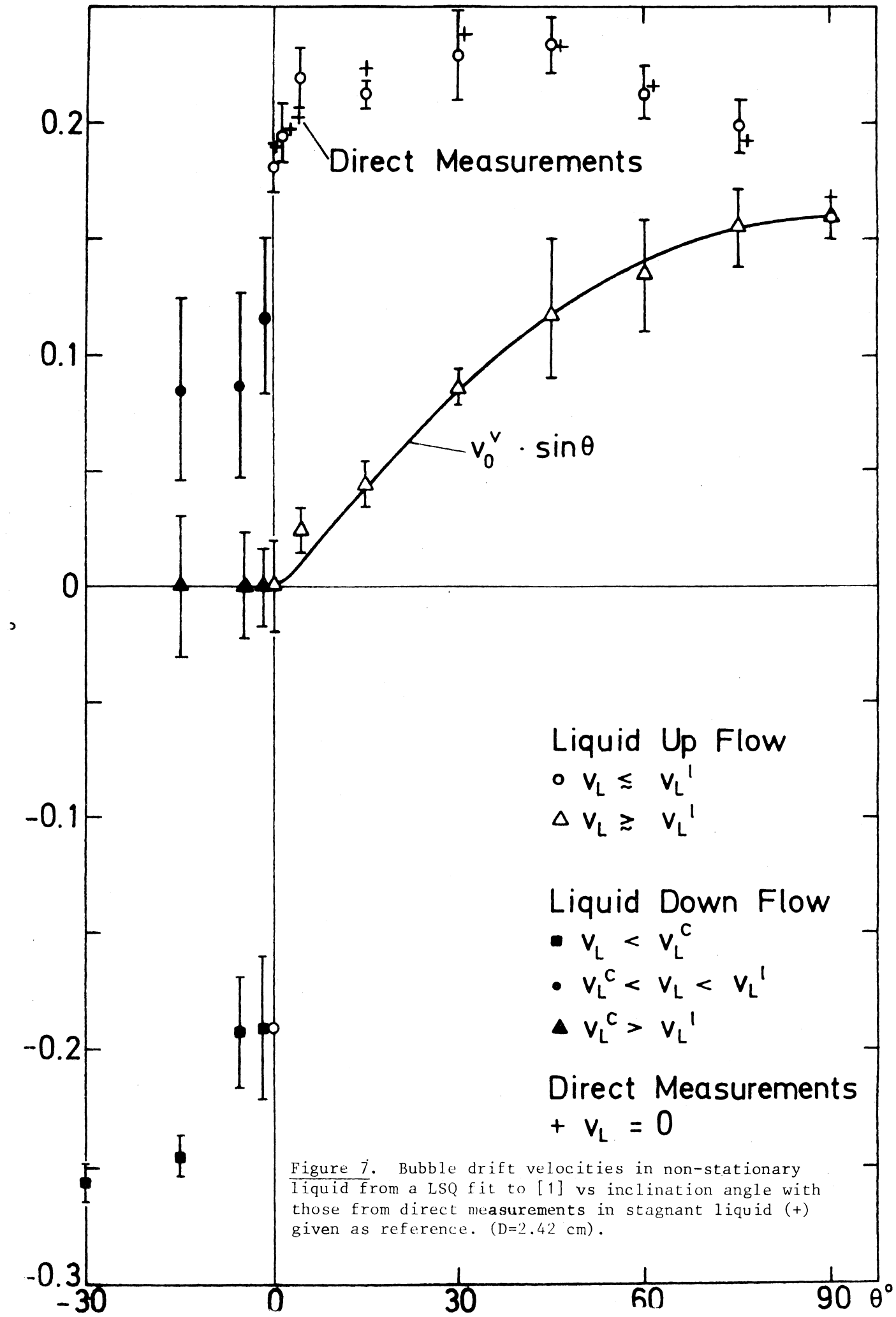

Figure 7. Bubble drift velocities in non-stationary liquid from a LSQ fit to [1] vs inclination angle with those from direct measurements in stagnant liquid (+) given as reference. (D=2.42 cm).

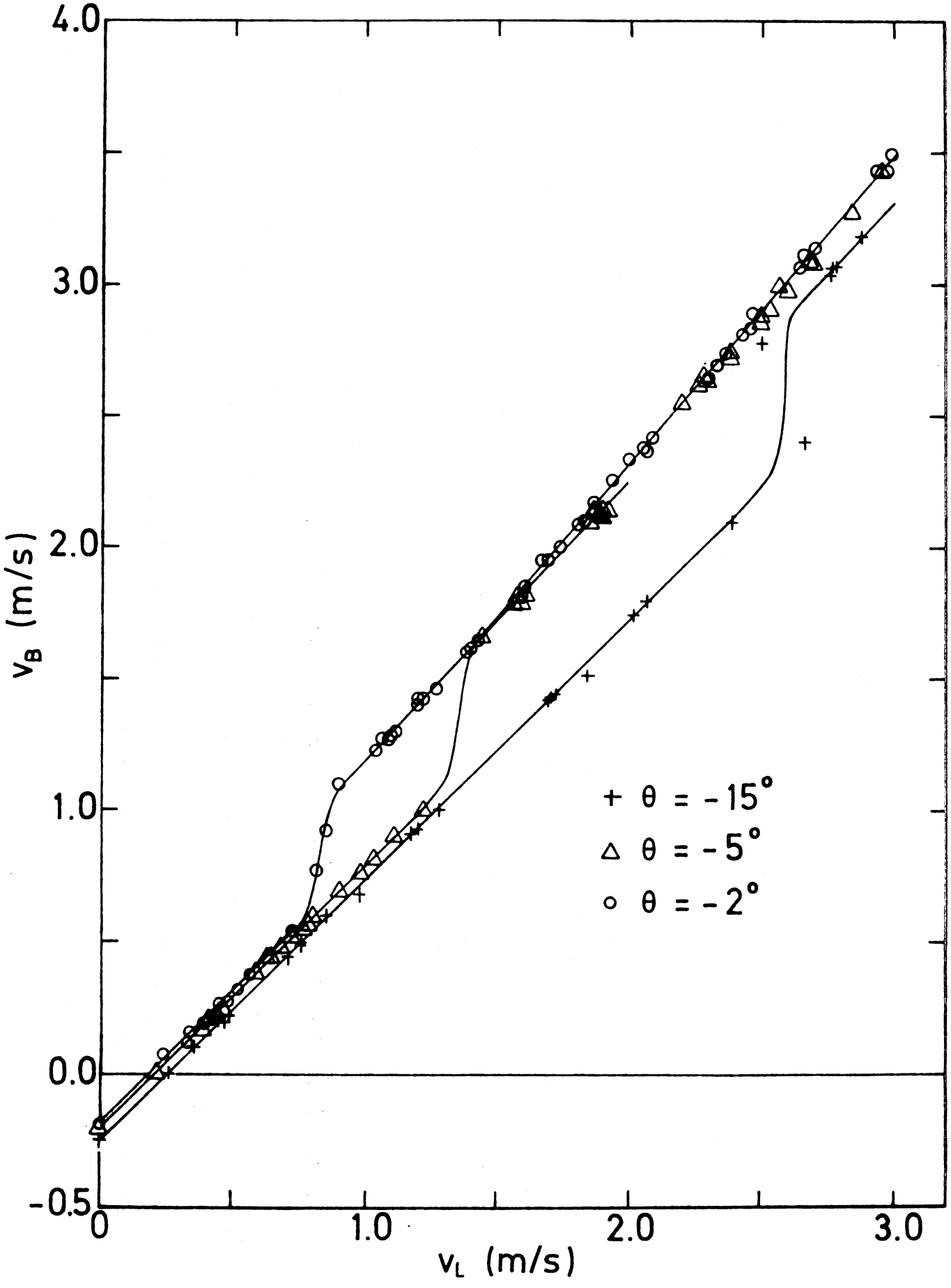

Figure 8. Measured bubble vs liquid velocity ($\theta<0$).

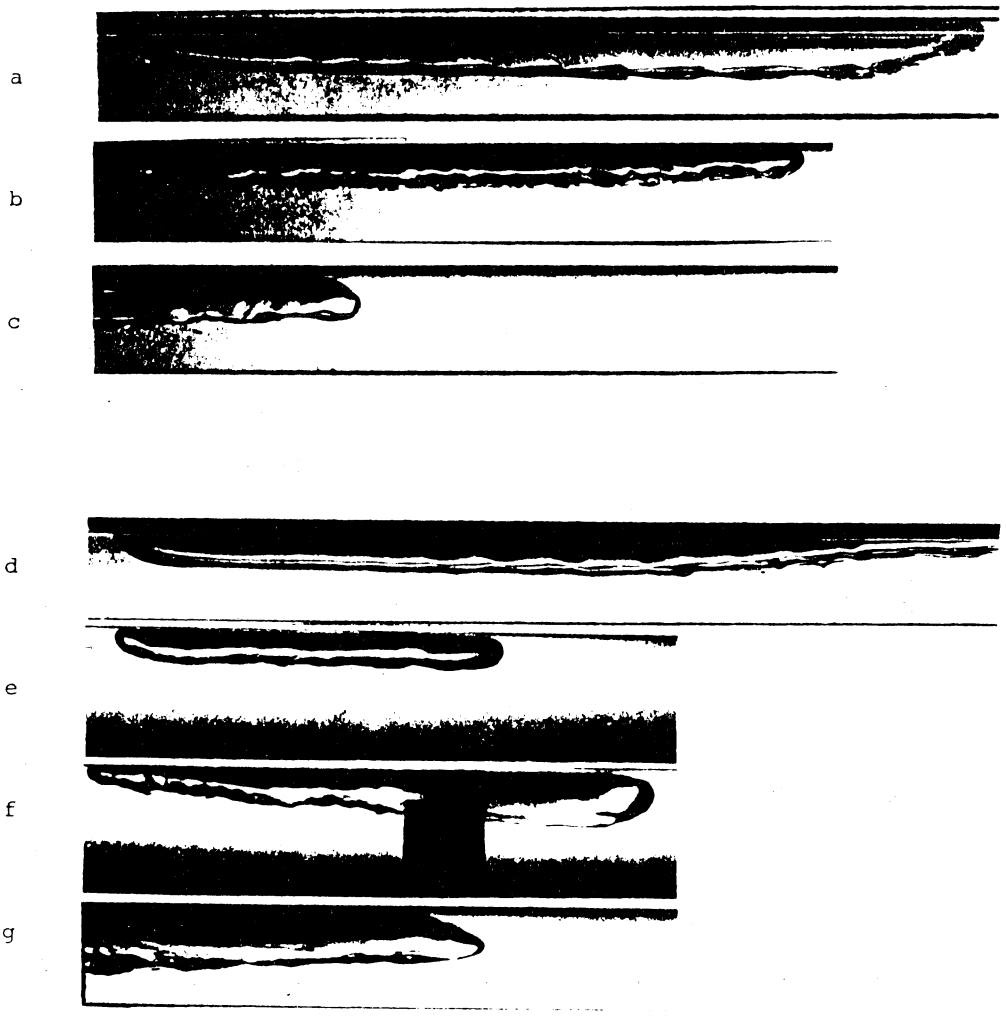

Figure 9. Illustration of the bubble turning process in liquid down flow
(a-c θ=-5°, d-g θ=-2°. a,d $v_L < v_L^c$, b,e $v_L \simeq v_L^c$, f $v_L > v_L^c$, c,g $v_L >> v_L^c$).

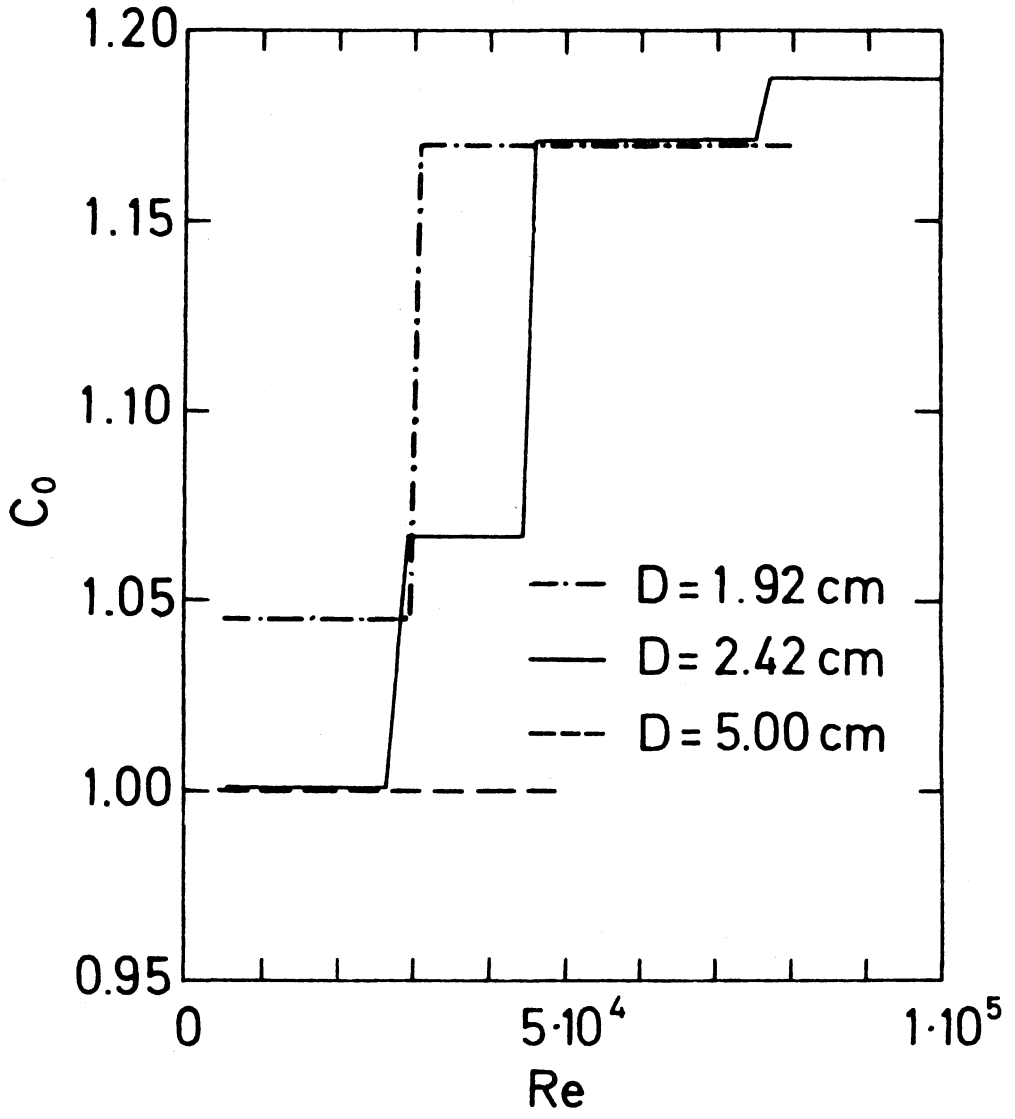

Figure 10. The coefficient C_0 vs Reynolds number for different tube diameters ($\theta=0^o$).

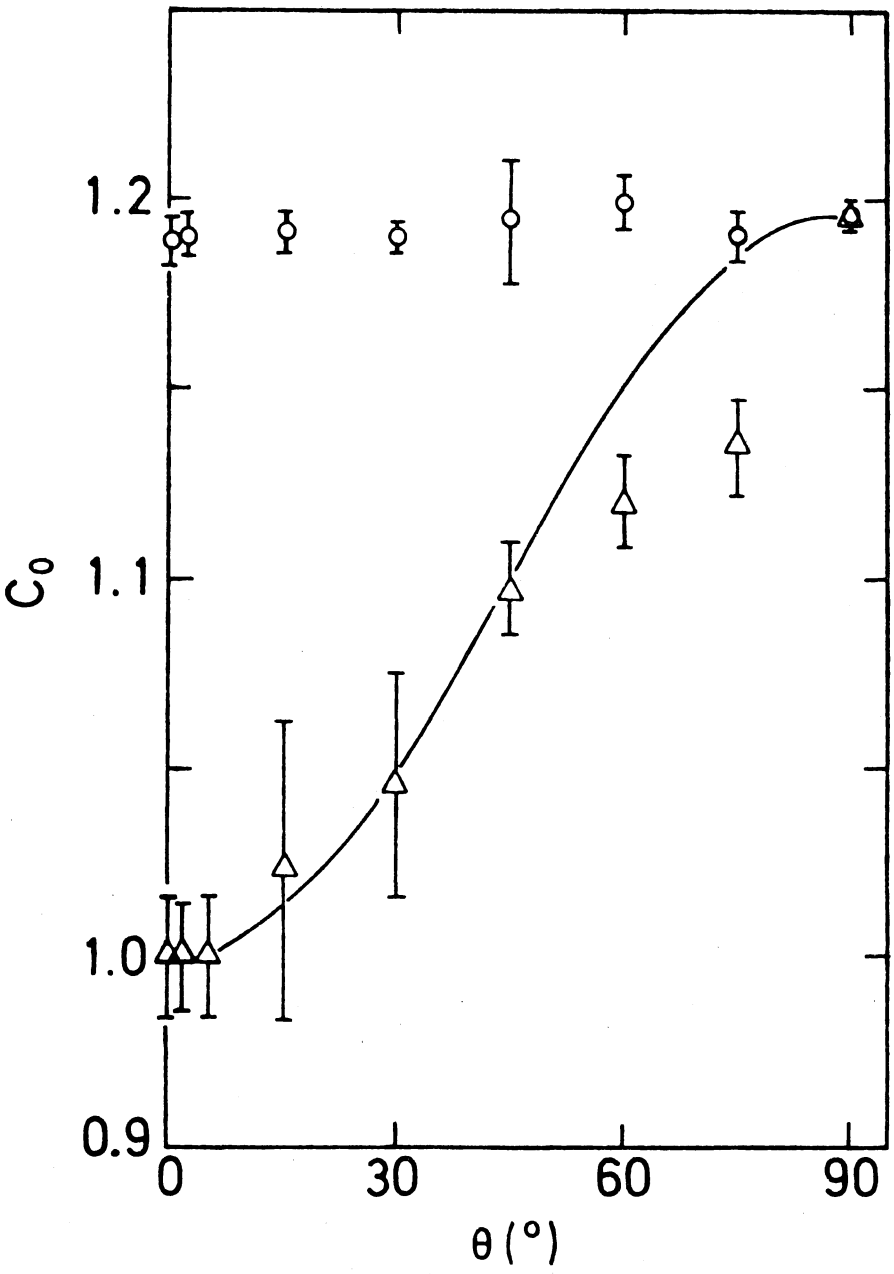

Figure 11. The coefficient C_0 vs inclination angle for the lowest (Δ) and highest (o) velocity intervals (D=2.42 cm, —— $C_0(\theta)=C_0(0^o)+[C_0(90^o)-C_0(0^o)]\cdot\sin^2\theta$).

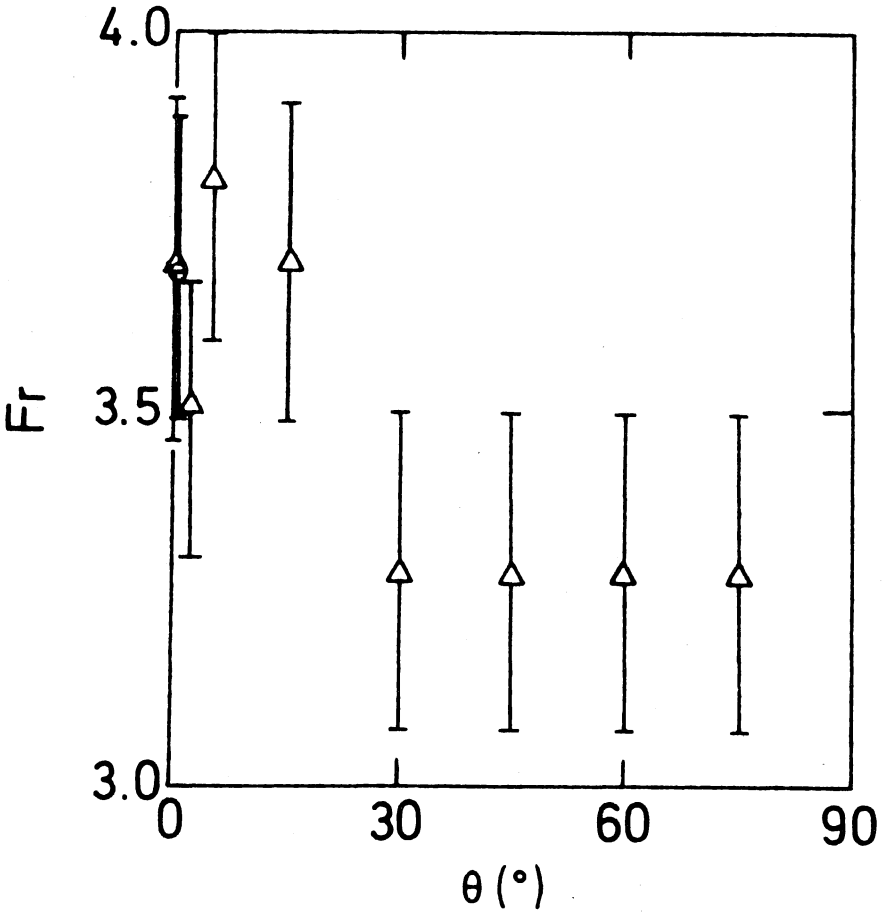

Figure 12. Froude number where transition to the highest C_0 occurs vs inclination angle (ΔD=2.42 cm, oD=1.92 cm).

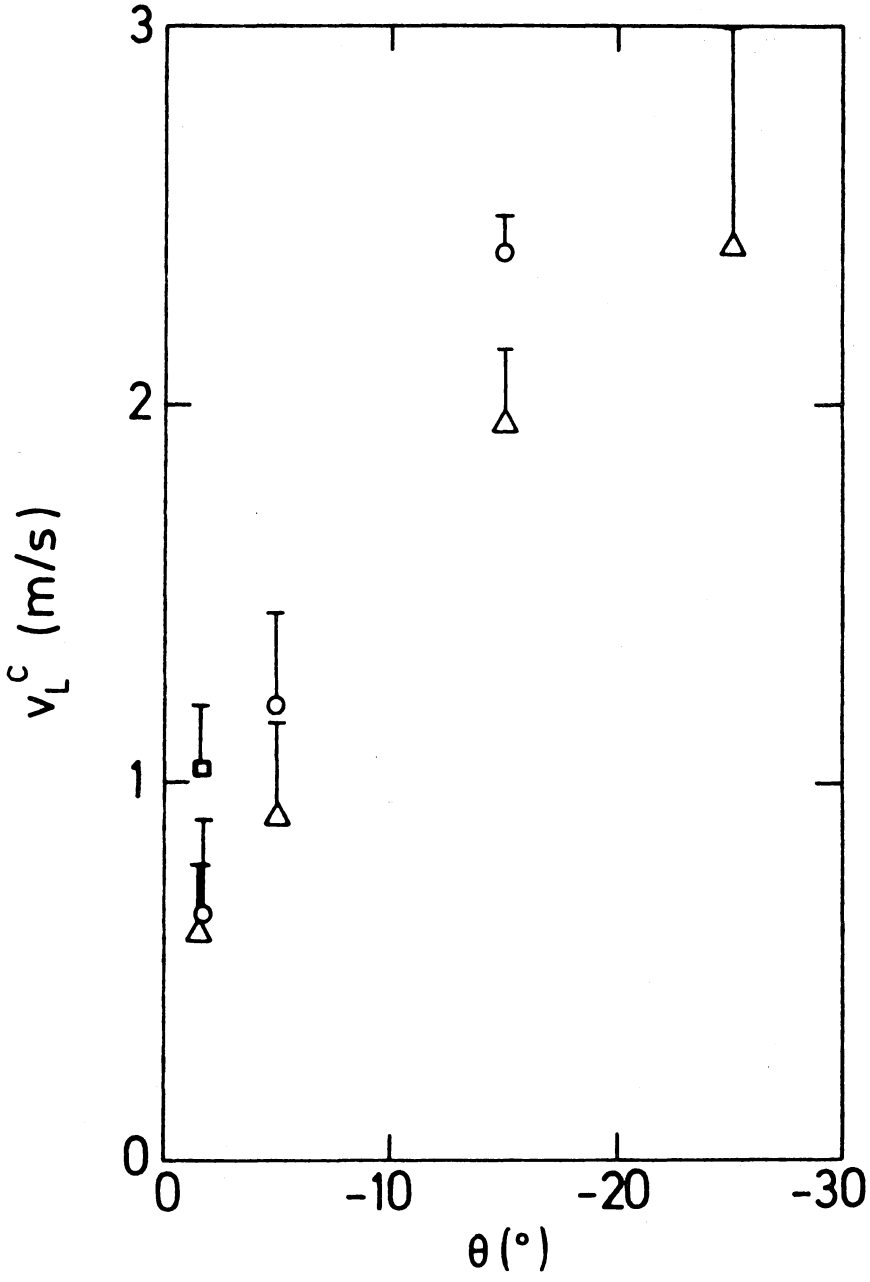

Figure 13. Critical average liquid velocities for bubble turning (□D=5 cm, oD=2.42 cm, ΔD=1.92 cm).

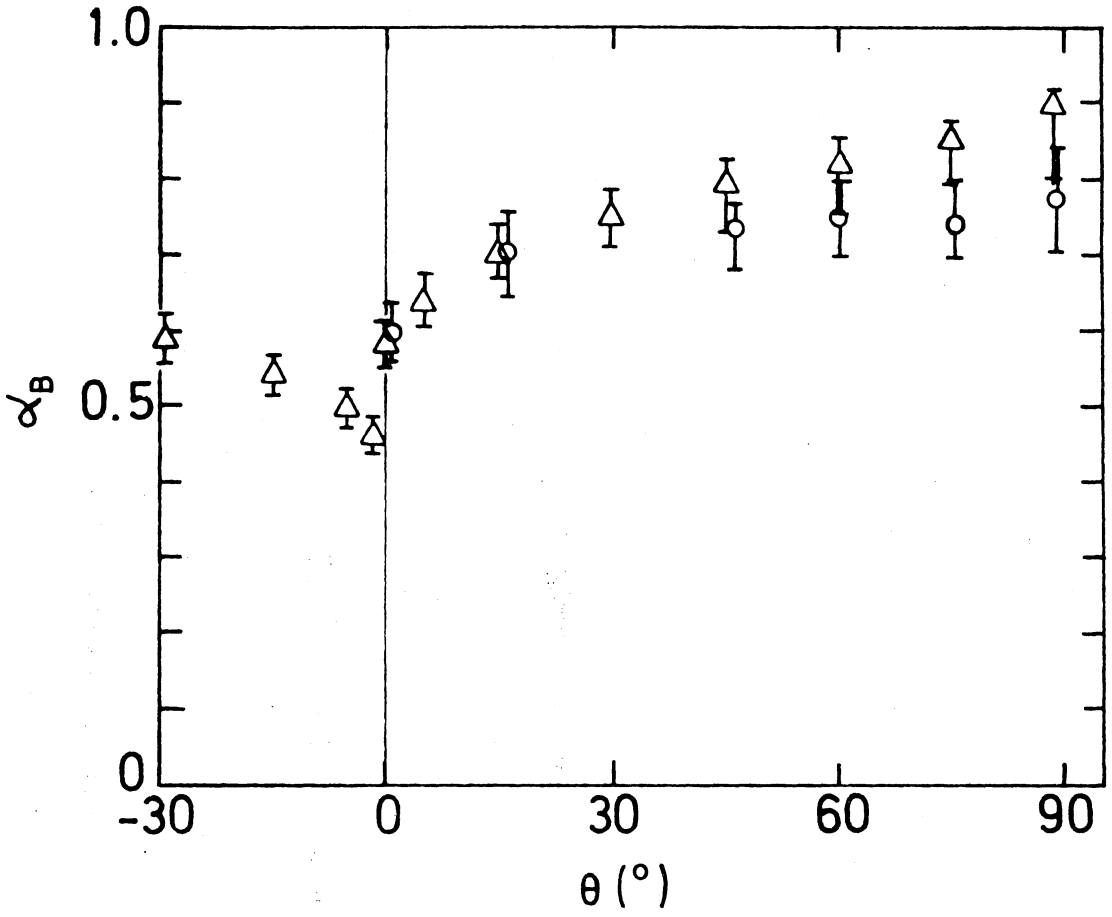

Figure 14. Measured asymptotic void fractions in the bubble for the lowest and highest liquid velocity intervals ($\Delta Fr \lesssim 2$, $oFr \gtrsim 3.5$, D=2.42 cm).

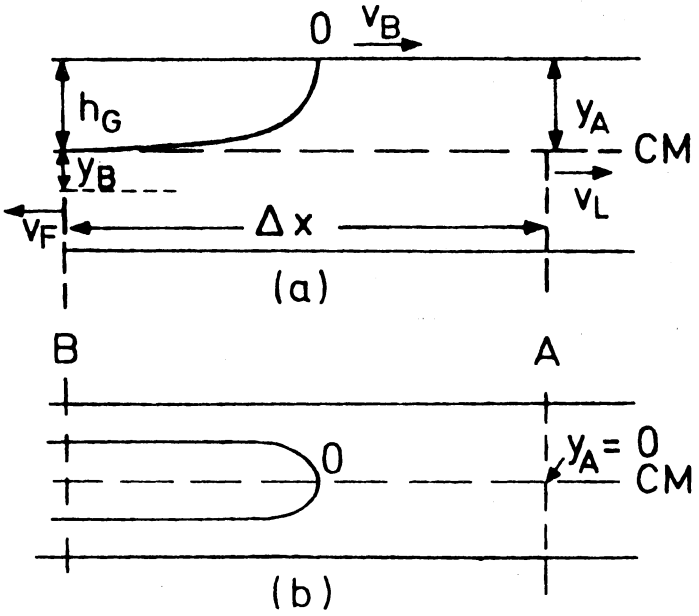

Figure 15. Schematic representation of a bubble in inclined flow (Fr<<1).

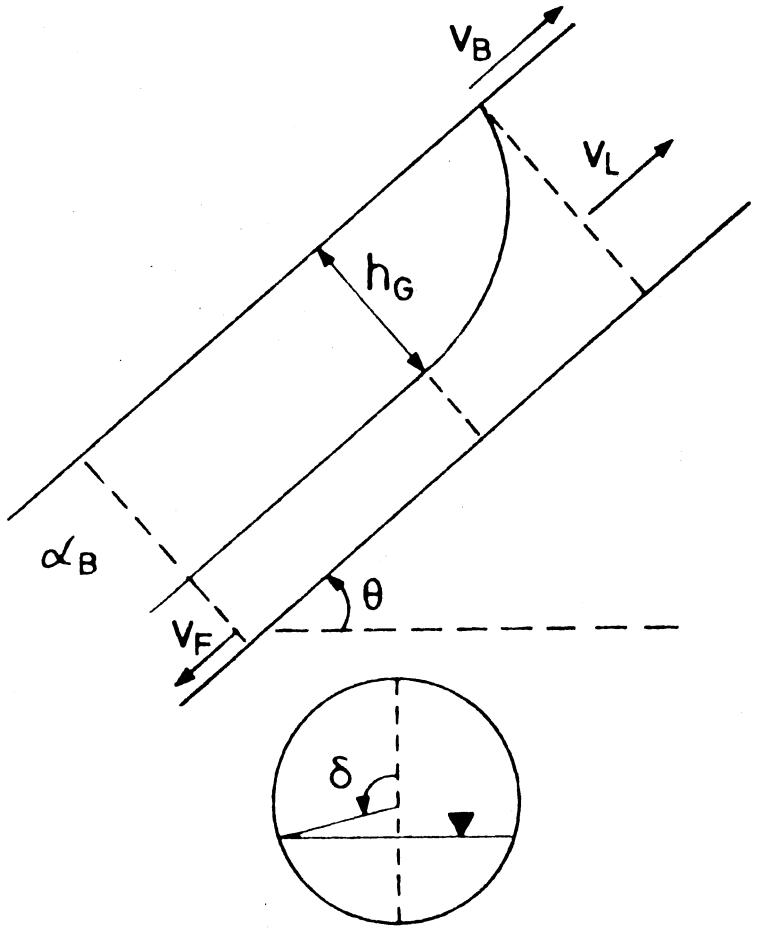

Figure 16. Schematic representation of a bubble in inclined flow (Fr<<1).

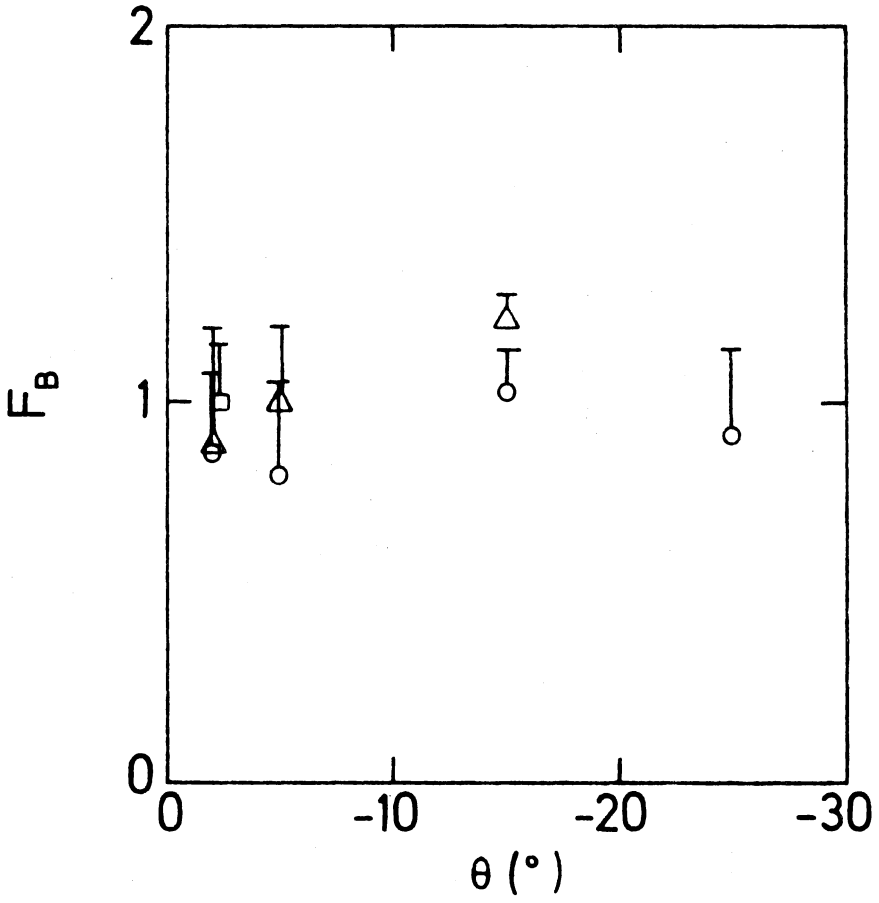

Figure 17. Measured bubble turning velocities represented by the F_B-number [17] (oD=1.92 cm, ΔD=2.42 cm, □D=5.00 cm).

NOMENCLATURE

A	Flow area, m^2
C_0	Distribution parameter
D	Tube diameter, m
g	Gravitational acceleration, m/s^2
h_f	Liquid or gas phase height in tube, m
K	Maximum to average liquid velocities
L	Bubble length, m
P	Pressure, N/m^2
Re	$\rho D v_L / \mu$ Liquid Reynolds number
S_f	Wetted perimeter, phase f, m
t	Time, s
T	Temperature, K
U	Superficial velocity, m/s
v	Velocity, m/s
v_0	Bubble rise velocity in stagnant liquid, m/s
x_j	Separation distance between transistor/diode pairs j-1,j

GREEK SYMBOLS

α	Void fraction
λ	Friction factor
μ	Viscosity, Ns/m^2
δ	Dry angle, rad
Δ	Uncertainty, or standard deviation
ρ	Density, kg/m^3
σ	Surface tension, N/m
Σ	$4\sigma/(g\rho_L D^2)$ Dimensionless surface tension parameter
θ	Inclination angle between the horizontal and the liquid flow direction, degrees
ϕ	Angle between diode/transistor axis and the horizontal, degrees

SUBSCRIPTS

B	Bubble
f	Phase
F	Liquid film
G	Gas phase
h	Horizontal
i	Interfacial
L	Liquid phase
r	Relative
s	Liquid in front of the bubble
$\star$	Dimensionless